Published in final edited form as:
Bone. 2007 April ; 40(4): 919–930.

EFFECT OF MECHANICAL STIMULI ON SKELETAL REGENERATION AROUND IMPLANTS

Philipp Leucht[1,2], **Jae-Beom Kim**[1], **Rima Wazen**[3], **Jennifer A. Currey**[4], **Antonio Nanci**[3], **John B. Brunski**[4], and **Jill A. Helms**[1]

1 *Department of Plastic and Reconstructive Surgery, Stanford University, Stanford, CA 94305, USA*

2 *Department of Trauma, Hand and Reconstructive Surgery, Johann-Wolfgang-Goethe University of Frankfurt/Main, 60590 Frankfurt/Main, Germany*

3 *Département de stomatologic, Faculté de médecine dentaire, Montréal, Québec, Canada H3C 3J7*

4 *Department of Biomedical Engineering, Rensselaer Polytechnic Institute, Troy, NY 12180, USA*

Abstract

Due to the aging population and the increasing need for total joint replacements, osseointegration is of a great interest for various clinical disciplines. Our objective was to investigate the molecular and cellular foundation that underlies this process. Here, we used an *in vivo* mouse model to study the cellular and molecular response in three distinct areas of unloaded implants: the periosteum, the gap between implant and cortical bone, and the marrow space. Our analyses began with the early phases of healing, and continued until the implants were completely osseointegrated. We investigated aspects of osseointegration ranging from vascularization, cell proliferation, differentiation, and bone remodeling. In doing so, we gained an understanding of the healing mechanisms of different skeletal tissues during unloaded implant osseointegration. To continue our analysis, we used a micromotion device to apply a defined physical stimulus to the implants, and in doing so, we dramatically enhanced bone formation in the peri-implant tissue. By comparing strain measurements with cellular and molecular analyses, we developed an understanding of the correlation between strain magnitudes and fate decisions of cells shaping the skeletal regenerate.

Keywords

implant; micromotion; strain; osseointegration; osteochondroprogenitor cell

Introduction

The skeleton is a structural, load-bearing system, and in this capacity the tissues comprising the skeleton must be capable of sensing mechanical stimuli in their local environment, interpreting these stimuli, and responding in a biologically appropriate fashion. Our ambition was to understand how skeletal progenitor cells respond to mechanical stimuli in a clinically relevant model of bone regeneration. To that end we developed a model of implant

Corresponding author: Jill A. Helms, 257 Campus Drive, PSRL Building, Stanford, CA 94305, USA, Phone: (650) 736-0300; Fax: (650) 736-4374, jhelms@stanford.edu

This work was funded by NIH grant: R01 EB000504-02.

osseointegration that enabled us to modulate the mechanical environment at the bone-implant interface and then examine on a molecular, cellular, and tissue level, how cells behaved in response to a defined mechanical stimuli.

Successful implant osseointegration and its clinical longevity depend upon the way mechanical stresses are transferred to the surrounding bone or tissue. This force transfer from the implant to the surrounding bone is influenced by the type of loading that occurs (i.e., intermittent, continuous), the bone-implant interface (i.e., direct contact or a gap interface), the length and diameter of the implant, the implant shape, the surface texture of the implant, and the quality and quantity of the surrounding bone [1–7]. Thus, multiple factors influence successful osseointegration and by understanding the most critical variables one may be able to optimize implant stabilization.

When an implant is placed into a tight-fitting hole, the bone-implant interface is composed of regions with direct bone-implant contact, and regions without direct contact and therefore a gap interface [8]. Biomechanical principles dictate that implant loading generates stress and strain fields, and the magnitude and quality of these stress and strain fields will vary, based on whether there is direct contact with the implant, or a gap interface [8,9]. Because these stresses and strains at the bone-implant interface are heterogeneous, it becomes more difficult to determine the nature of the relationship between strain fields and cell differentiation.

In our experimental model, we sought to simplify the architecture of the initial implant interface in order to better address the question of how skeletal progenitor cells in the interfacial region respond to mechanical strain *in vivo*. Instead of creating a heterogeneous interface composed of regions with direct bone-implant contact and regions with gaps, we created only a gap-type interface by placing a 0.5 mm implant in a 0.8 mm hole. The implant was stabilized in this oversized hole by an external device, which was also the means by which a defined micromotion was later delivered to the implant. This type of implant/hole geometry, together with the external device, allowed us to selectively investigate how the skeleton regenerates around an implant, and how micromotion and the associated strain fields affected the differentiation of skeletal progenitor cells that populated the implant site.

Materials and Methods

Surgical procedure, implant design and micromotion system

All experiments were performed in accordance with Stanford University and Rensselaer Polytechnic Institute Animal Care and Use Committee guidelines. Forty-five three-month old, male CD-1 mice were purchased from Charles River Laboratories, Inc. (Wilmington, MA). Animals were housed in a light- and temperature-controlled environment and given food and water ad libitum.

The mouse model involved two unique features: first, placement of a 0.5 mm-diameter, surface-characterized polymer pin-shaped implant (Poly(L-lactide-co-D,L-lactide), i.e., 70% L-lactide and 30% D,L-lactide, material grade LR706, Midwest Plastics, MN and Medical Micro Machining, Inc., Simi Valley, CA) in a 0.8 mm diameter drill hole in the mouse tibia in order to create a pure gap interface; and second, a micromotion device ensuring control over stabilization or motion of the implant within the wound site. The surgical installation and further details of the implant system are described next.

Mice were anaesthetized with an intraperitoneal injection of Ketamine (80mg/kg) and Xylazine (16mg/kg) [10]. An incision was made over the right anterior-proximal tibia and the tibial surface was exposed whilst preserving the periosteal surface. Two screw holes were drilled through both cortices with a high-speed dental engine (20.000 rpm) using a 0.5 mm drill bit

(Drill Bit City, Chicago, IL); these holes accepted proximal and distal fixation screws (0.6 mm diameter titanium alloy "Retopins", NTI Kahla GmbH, Germany) to hold down the bone plate of the micromotion device. The bone plate was made of Delrin® polymer (Medical Micro Machining, Inc., Simi Valley, CA); the plate's length and width were 5 mm × 2.15 mm, and its center column was 2 mm in diameter and 1.83 mm tall (Fig. 1). Using the bore of the center column of the bone plate for guidance, the mono-cortical implant hole was drilled using a 0.8 mm drill bit. Afterward, the implant, whose main diameter was 0.8 mm and whose 0.5 mm-diameter tip included two defined ridges, was introduced into the hole. A silicone rubber o-ring (Apple Rubber Products Inc., Lancaster, New York), with an inner diameter of 0.81 mm, a cross section of 0.6096 mm, and a durometer (Shore A scale) of 40, was placed between the top head of the implant and the center column of the Delrin® bone plate. A cap was screwed onto the center column of the bone plate to prevent implant motion when the mouse was allowed to ambulate freely in its cage. Finally, the wounds were closed with non-absorbable sutures around the center column of the Delrin® plate. By using the above mentioned device, bone regeneration around the implant can be studied in: a) a stable implant environment with the absence of implant motion; and b) a mechanically-perturbed environment, associated with controlled axial implant micromotion (described later). Following surgery, mice received subcutaneous injections of buprenorphine (0.05–0.1 mg/kg) [10] for analgesia and were allowed to ambulate freely. No antibiotics were given to the operated animals. Five mice were sacrificed at each of the following time points: 3, 7, 14, 21 and 28 days post-surgery.

Tissue processing, histology and immunohistochemistry

The right limbs were dissected, skinned and then fixed in 4% paraformaldehyde overnight. Decalcification was achieved by introducing the samples into 19% EDTA-2Na solution for ten days at 4°C. After demineralization, the implant device was gently pulled out of the bone. Specimens were dehydrated through an ascending ethanol series prior to paraffin embedding. Eight micron-thick longitudinal sections were cut and collected on Superfrost-plus slides for histology using a modification of Movat's Pentachrome staining [11]. Adjacent sections were analyzed by PECAM-1 (BD Pharmingen) antibody staining as previously described [12]. Using this protocol, we visualized mesenchymal stem cells by using an antibody for the stem cell-associated antigen (Sca-1) (BD Pharmingen). Proliferating cells were detected by immunohistochemistry for PCNA (Proliferating Cell Nuclear Antigen) (Zymed). The intranuclear PCNA protein plays a role in the initiation of cell proliferation by mediating DNA polymerase. PCNA expression has a broad correlation with mitotic activity and therefore can be used as a marker for cell proliferation. Thus, the sections were incubated with biotinylated mouse anti-proliferating cell nuclear antigen antibodies (PC-10) at room temperature for 45 minutes. Streptavidin-peroxidase was used as a signal generator, diaminobenzidine (DAB) (Zymed) as a chromogen to stain PCNA-positive nuclei dark brown.

In situ hybridization

Hybridization was performed using Digoxigenin-labeled probes synthesized complementary to mouse cDNAs for *col I, col II*, and *sox9* as previously described [13]. In detail, the relevant mRNAs for in situ hybridization were prepared using sequence-specific primers and polymerase chain reaction. Tissue sections were incubated in hybridization buffer (Ambion Corporation) containing Digoxigenin-labeled riboprobe at an approximate concentration of 0.2–0.3 μg/ml probe per kilobase of probe complexity. Non-specifically bound probe was hydrolyzed with RNase A, and final washes were carried out at high stringency (0.2× SSC, 52°C). For color detection, slides were blocked with 10% sheep serum and Levamisole, and developed using Nitro blue tetrazolium chloride (NBT) and 5-Bromo-4-chloro-3-indolyl phosphate (BCIP; Roche, Indianapolis, IN). After developing, the slides were cover-slipped with aqueous mounting medium.

Micromotion

Micromotion of the implant was generated by a separate hand-activated system that can be firmly connected to the cap attached to the center column of the bone plate while delivering short bouts of micromotion (e.g., last about 1 minute). This system consisted of: a) a linear variable differential transducer, or LVDT (TransTek Inc., Ellington, Connecticut Model #0240-00000); b) a load cell (Honeywell Sensotec, Columbus, Ohio Model #11) with a load range of 0 to 2.27 kg; and c) a core for the LVDT, one end of which was connected to the load cell, and the other end consisting of a small (~1 mm) tip that could pass through a 1.1 mm-diameter hole in the cap on the center column of the bone plate in order to produce axial motion of the implant. Data were collected at 200 Hz sampling rate via a DaqBook system (iO Tech Inc., Cleveland, Ohio). With this series connection of LVDT and load cell, it was possible to produce and measure axial motion of the implant plus the force required producing this motion. A part of the force measured by the load cell compresses the rubber o-ring (of known stiffness), while the remainder is due to the resistance of the interfacial tissue.

Strain simulation

The micromotion device was attached to a wood dowel, with the test implant residing in a 0.8 mm diameter hole filled with rubber (ReproRubber®, Small Parts, Inc., Miami Lakes, FL) mixed with tantalum powder with particle size of approximately 50 microns. The rubber interface with tantalum powder was designed to provide radiopaque markers that are visible in a micro-CT image for the purpose of strain analysis. Following curing of the rubber, the wood dowel was mounted in a micro-CT scanner [Physiological Imaging Research, Mayo Clinic, Rochester, MN]. Micro-CT scans were obtained before and after implant displacement of approximately 150 μm in the interface. The micro-CT stage allowed 360° rotation of the wood dowel about its long axis in small angular steps of ~0.5°. Images were 1024 × 1024 pixels with a pixel size of 5.959 μm and were further processed in Analyze software. The center plane of the implant (the area of interest for the strain analyses) was found by stepping through the slices (6 μm apart), to locate the implant at its widest diameter. Images, before and after displacement, were then analyzed via DISMAP [25] to determine strain fields in the gap region around the implant.

Results

All implants were placed in murine tibiae so that only the medial cortex was penetrated and the far cortex was left intact (Fig. 1A, B); we describe this as a mono-cortical defect. Healing was uneventful following device installation. The motion devices were stable, as assessed by tactile and visual inspection at the time of sacrifice. Furthermore, we did not detect signs of inflammation or infection at any implant site during the course of the study.

Our primary goal was to understand the molecular and cellular regulation of osseointegration. To that end, we examined unloaded implants at 3, 7, 14, 21, and 28 days post-surgery in order to determine how cells behaved when they were in a motion-neutral environment. We then compared these baseline data with the behavior of cells adjacent to a loaded implant. We focused our attention on three sites around each implant: the periosteum adjacent to the implant, the gap between the cortical drill edge and the implant itself, and the bone marrow-implant interface. We chose these three locations because each potentially contributes to implant stabilization and therefore has a direct influence on the clinical outcome.

Periosteum accomplishes rapid implant stabilization through cartilage intermediate

Three days after placing an implant into the tibia, the adjacent periosteum exhibited a marked reaction to the injury; specifically, the cambial layer of the periosteum increased almost ten-fold as compared to the cambial layer of uninjured periostea (n=5; Fig. 2A, B). This exuberant

periosteal reaction is reminiscent of the response of injured periosteum [14,15]. Therefore we tested if this periosteal reaction was simply caused by the implant surgery, or by placing the motion device onto the tibial surface. We reproduced all of the surgical steps without placing the motion device, and this resulted in the same proliferative effect (data not shown). Therefore, we concluded that the proliferative periosteal reaction was not induced by the placement of the motion device, but instead was triggered by the injury of the tibia in conjunction with implant placement.

We also noted that while the dimensions of the cambial layer were increased, the fibrous, outer layer of the periosteum remained unchanged (Fig. 2B). To understand the basis for this selective expansion of the cambial layer, we examined adjacent tissue sections for evidence of vascularization, cell proliferation and differentiation. We noted that both cambial and fibrous periosteal layers were evenly vascularized as evidenced by PECAM immunostaining (Fig. 2C). Proliferation activity, assayed by PCNA immunohistochemistry, was restricted exclusively to the cambial layer (Fig. 2D). These cellular assays indicated that the injured periosteum was rapidly re-vascularized after injury. We next set out to determine the state of differentiation of the periosteal cells.

We used *in situ* hybridization to identify the spatial distribution of osteogenic and chondrogenic genes. For example, *col I* is typically viewed as a marker of differentiated osteoblasts [16] but its expression extends to mesenchymal cells committed to an osteoblast fate [17]. On the other hand, the transcription factor *sox9* directly regulates *col II* expression [18] and while both are expressed by differentiated chondrocytes [19], these genes are also expressed by progenitor cells committed to a chondrogenic lineage [19]. Our *in situ* hybridization analyses revealed that cambial cells concomitantly expressed *col I*, *col II*, and *sox9* (Fig. 2E-G). The co-localization of Sca-1 immunostaining (Fig. 2H) with these gene expression patterns indicated that cells in the cambial layer adjacent to the implant shared a number of characteristics associated with progenitor cells that had the capacity to differentiate into either chondrocytes or osteoblasts.

Seven days after implant placement in an unloaded environment, the periosteum exhibited an unexpected amount of hypertrophic cartilage (Fig. 2I). Typically, hypertrophic cartilage is thought to form in areas of low oxygen tension, which is brought about by decreased vascularization [20] associated with motion at the site of injury [21]. This was unlikely to be the primary explanation for the presence of cartilage in the periosteum, however, since we had seen abundant PECAM staining at earlier time points (Fig. 2C). Regardless of the cause, by post-surgical day 14 the hypertrophic cartilage in the injured periosteum had undergone vascular invasion (Fig. 2J, K), the first islands of osseous matrix were evident, and the tissue was rapidly being remodeled by TRAP positive osteoclasts (Fig. 2L). The majority of cells in the periosteal proliferation zone were *col I* positive (Fig. 2M). By post-surgical day 28, the cortical bone had dramatically increased its thickness and a distinction between the former cortical surface and the new periosteal-derived bone was hardly recognizable (Fig. 2N). The only noticeable difference was the organization of the bone matrix, which appeared lamellar in the pre-existing bone and was less organized in the newly formed bone. In conclusion, the periosteal compartment responds to a stable implant by following the program of endochondral bone formation. In this manner, rapid stabilization of the stable implant occurred through a cartilage intermediate, which eventually was replaced by a mineralized bone matrix during the course of osseointegration.

Bridging of the cortical gap occurs by intramembranous bone formation

We created gap-type interfaces in all of our implants by placing 0.5 mm implants into 0.8 mm holes, leaving a gap of ~ 0.15 mm in thickness surrounding the implant. All implants were immediately stabilized by our fixation device to prevent unintended motion (Fig. 1A, B). At

post-surgical day 3, the gap space was filled with spindle-shaped fibroblasts (Fig. 3A), PCNA-positive, proliferating cells (Fig. 3B), and PECAM-expressing endothelial cells that started assembling to a tubular structure (Fig. 3C). In the gap region, *col I* expressing cells were predominantly located at the implant interface, with an accumulation around the circumferential ridge (Fig. 3D). Within 7d, new bone had almost occupied the entire gap region (Fig. 3E). Abundant vascularization was evident (Fig. 3F) and *col I*-positive cells lined the new osteogenic matrix (Fig. 3G). These two observations indicated that new bone formation was closely associated with a strong vascular response at the implant site. Few, if any, TRAP positive osteoclasts were detectable at d7 despite the presence of the new bone matrix (Fig. 3H). Bone in the gap region continued to mature and undergo osteoclast mediated remodeling at the day 14 time point (arrows, Fig. 3I, J) and post-surgical day 21 (data not shown). After 28 days, we found that the newly formed bone matrix was fully integrated with the cortical drill edges (Fig. 3K), which was achieved in large part through extensive TRAP-positive osteoclast remodeling (Fig. 3L). Thus, osseointegration in the gap region started after osteochondroprogenitor cells had proliferated and a vascular network was established. In contrast to the periosteum, where endochondral bone formation took place, the gap region was filled with bone by the process of intramembranous ossification.

The bone marrow cavity exhibits the slowest reaction to implant placement

Perhaps the least dramatic tissue transformation occurred in the marrow cavity in response to implant placement. Three days post-surgery, bone marrow cells adjacent to the implant appeared histologically indistinguishable from marrow cells located at a distance from the implant (Fig. 4A) and yet there was clear evidence of localized cell proliferation adjacent to the implant (Fig. 4B). *Col I* expression overlapped with this localized domain of cell proliferation (Fig. 4C), which suggested that a subset of marrow cells were in the process of committing to an osteogenic fate. At post-surgical day 7, cells at the implant-bone marrow interface still exhibited the fibroblast-like phenotype, with no signs of bone matrix deposition (n=7, Fig. 4D). In contrast to the periosteum and the gap area, vascular invasion into the wound site did not occur until day 7 (Fig. 4E). The expression pattern of the osteoblast marker *col I*, which was broad at day 3, was reduced to a thin band around the implant (Fig. 4F).

By post-surgical 14d, however, bone formation had surrounded the implant (Fig. 4G). Immediately after the onset of osteogenesis, TRAP positive osteoclasts started remodeling the rough sheath (Fig. 4H). *Col I* expression at this time point was restricted to cells which were directly attached to the newly deposited matrix (Fig. 4I). This bony encasement persisted in the marrow space; 28d post-surgery a well organized, lamellar coating encapsulated the implant on all sides (Fig. 4J). The region was largely devoid of TRAP positive osteoclasts (Fig. 4K), suggesting that the bony encasement had finalized its organization.

In conclusion, osseointegration of the implant in the bone marrow cavity occurred by intramembranous bone formation and this osteogenesis was not influenced by the shape of the implant, i.e. side of the implant or tip.

Mechanical stimuli enhance and accelerate osteogenesis

To gain insights into the molecular and cellular *in vivo* responses of tissues to physical stimuli associated with implant osseointegration, we employed our micromotion device to allow the delivery of a defined 150 μm axial displacement of the implant. Based on parameters established by other investigators [22–24] we applied the loading protocol on a daily basis with a frequency of 1.0 Hz, a duration of 60 sec for our initial study. In order to directly compare results from the stable implant data (Figs. 2–4) with implants that were subjected to motion, we harvested tissues at the same time points for our molecular, cellular, and histological analyses. Collectively, these assays revealed a dramatic change in cell behavior at almost all

implant surfaces examined at post-surgical day 7(Fig. 5A, B). We were initially surprised to see that the periosteum was not drastically altered by implant loading; cambial cells in the periosteum still proliferated and eventually differentiated into chondrocytes (Fig. 5C, D). The gap region, however, exhibited a radical adjustment in response to motion; at post-surgical day 7, we noted exuberant bone formation that filled the proximal and distal gap regions (Fig. 5E, F; also see Fig. 3E). A histological assessment of the gap regions indicated that the amount of new bone that formed by post-surgical day 7 in the motion cases was equivalent to the amount of new bone that formed by d14 in the stable implants (compare Fig. 5F with Fig. 3I).

Cells in the bone marrow cavity exhibited the most robust response to implant motion. Cells that in stable cases had maintained a fibroblastic morphology for at least 7d (Fig. 4A, D) now rapidly differentiated into osteoblasts by post-surgical day 7. And while relatively little bone matrix was evident in the stable cases at post-surgical day 7, bone marrow cells in the motion cases had laid down a mineralized matrix (n=8; Fig. 5G, H).

Strain fields shape the skeletal regenerate

We reasoned that due to the deliberately-chosen geometry of our implant, with its two circumferential ridges and its blunt base acting as strain concentrators, axial implant displacement would create distinct strain fields that would vary spatially in the interface. Our goal was to explore relationships between the strain field around the implant and the biological cellular response. Strain measurements *in vivo* are difficult to assess, because the material properties of the wound site change rapidly during the first days of healing. In order to circumvent this caveat, we created an *in vitro* simulation of the interface with analogous material properties as the early fibrin-rich blood clot that occupies the wound site. Also, we applied the same displacement to the implant in the simulation that we had recorded during our *in vivo* experiment (Fig. 6I). We took micro-CT images before and after implant displacement of 150 μm, and subjected the images to strain analyses using digital-image correlation [25]. By comparing the histology of the implant site 7 days after implant placement and motion with the strain measurements from our *in vitro* experiments, we investigated the correlation between the physical stimulus and the biological response. We found that areas of bone matrix deposition around the implant matched with areas of moderate values of effective strains (e.g., 0.25 to 0.50). These strain fields corresponded to regions near the smooth sides of our implant (between the ridges; Fig. 6A, B).

Next, we analyzed two high-strain regions around the implant and found that the tissue around the circumferential ridge was composed of bone matrix, except in a small area, where axial implant displacement of 150 μm caused the highest strains (e.g., 1–2 effective strain; Fig. 6C, D and Fig. 7B). The expression of *col 1* in this high strain area suggested that osteochondroprogenitor cells were present or had migrated to this site, but differentiation into osteoblasts did not occur (Fig. 6E).

The tissue at the base of the implant was another site of high strain, and the cellular reaction was similar: osteochondroprogenitor cells occupied the site but failed to differentiate into osteoblasts (Fig. 6F,H). This region was, however, surrounded by abundant bone matrix indicating that osteoblast differentiation only failed in areas of excessively large strains. In areas of moderate strain farther from the implant, osteoblast differentiation proceeded normally (Fig. 6G, H). In the area between the two circumferential ridges, where lower effective strains predominated, osteoblast differentiation and bone matrix deposition took place in close proximity to the implant surface (Fig. 7A,B). Overall, our histological, molecular and histomorphometric analyses demonstrate a tight correlation between strain magnitudes and the fate of osteochondroprogenitor cells during interfacial healing.

Discussion

Why do periosteal progenitor cells undergo endochondral ossification?

One of the earliest responses to skeletal injury is seen in the periosteum [14,15] and the viability of the periosteum is critically important to the process of bone repair. Bone fractures that disrupt the periosteum oftentimes impede the blood supply to the wound site; consequently, the skeletal injury is slower to heal. Removing the periosteum also compromises healing through a similar mechanism [26]. Clinical studies suggest that when an implant is placed into bone, the periosteum reacts by proliferation, which enhances bone formation in the early days after implant placement and thus provides initial stabilization to the implant [27]. The program by which bone formed in the periosteal compartment, however, was not clear [27].

We used a variety of molecular, cellular, and histological assays to examine in more detail the response of the periosteum to injury, to injury coupled with implant placement, and to injury coupled with placement and then micromotion of the implant. We confirmed the previously reported cell proliferation, and in addition noted that this proliferative response was limited to the cambial layer of the periosteum (Fig. 2). A majority of progenitor cells residing in the cambial layer differentiated into chondrocytes, which were then removed and replaced by bone through the program of endochondral ossification.

We wondered which cellular and molecular events controlled the decision of these periosteal progenitor cells to differentiate into cartilage. Some authors state that disruption of the vascular network, with its accompanying hypoxia, favors the differentiation of osteochondroprogenitor cells towards a chondrogenic lineage [28–30]. This explanation, however, does not match our observation of multiple small PECAM-positive endothelial cells, and vessels filled with red blood cells, in the cambial layer as well as in the fibrous layer of the periosteum within 72h of surgery (Fig. 2). All of the periosteal layers appeared to be highly vascularized early in the repair process, so it is unlikely that the cartilage formed only as a consequence of prolonged hypoxia in the region.

Another possible explanation for the cartilage formation in the periosteum is that dead osteocytes, which are embedded into the cortical bone close to the injury site, block the nutrient and oxygen supply for the periosteal osteoblast [31]; consequently, periosteal cells may differentiate into chondrocytes as a result of this starvation. Alternatively, osteocyte cell death may disrupt the molecular signaling cascade, such that osteogenic agonists are less represented and as a result, periosteal osteoprogenitor cells differentiate into chondrocytes instead of osteoblasts [32–39]. We noted empty lacunae (a sign of dead osteocytes) in the cortex close to the implant site, but found that this area did not correspond to the size of the periosteal cartilage reaction. Instead, the cartilage domain was at least twice the size of the region of cortical bone containing dead osteocytes. Thus, it is unlikely that the sole explanation for cartilage formation is due to an absence of osteogenic stimuli from cortical osteocytes, as has been suggested [31].

A third possible explanation for the chondrogenic response of the regenerating periosteum is that its mechanical strain environment is altered by injury and this new environment favors the activation of chondrogenesis [9,33,40]. We tested the possibility that implant placement, or the apparatus associated with implant placement itself, created a unique mechanical environment that favored the formation of cartilage. We found, however, that cartilage formation was evident even in cases where the implant apparatus was not used.

An alternative hypothesis is suggested by finite element models, which predict that cell proliferation can create regions of increased hydrostatic pressure and that hydrostatic pressure favors a chondrogenic fate [41,42,43]. We found evidence of selective cell proliferation in the

cambial (inner) layer of the periosteum and relatively little proliferation in the fibrous (outer) layer. When these cellular data are considered along with the finite element model, then it is possible that rapidly-dividing cells in the cambial layer experience pressure because they are surrounded and restrained by a "belt" of more slowly-dividing cells in the fibrous layer. We currently do not have a reliable method to quantify – or even reliably identify – such micro-mechanical environments. Nonetheless, it may be possible to test whether the fibrous layer is under tension by simply measuring relaxation of this layer following longitudinal incision.

Is bone formation in the marrow cavity dependent upon micromotion?

When the human organism senses a foreign body it institutes an initial inflammation with the intention to remove the invading entity. If this acute inflammatory response turns into a chronic state, one of the body's goals is to encase the foreign material in order to isolate it from surrounding tissue. One might think of an implant as a foreign body, albeit a sterile one; nevertheless an implant is not completely inert and thus it can induce a rejection response.

The skeleton's response to a foreign body may be encapsulation by a bony matrix. We know from other studies [24,9,8] that in addition to the physiological urge to encase an implant, the human skeleton may be able to sense the mechanical environment around an implant and – perhaps according to the effective strain field – decide to build a bony or a fibrous encapsulation. Our study suggests that when implant micromotion creates effective strains on the order of 0.25–0.50, bony encapsulation occurs. Conversely, when effective strains exceed 0.50, bone matrix deposition is blocked and a fibrous, cell-rich tissue occupies the site. Our rigid micromotion device guarantees stability of an implant and thus results in a strain-free environment. As a consequence, osteochondroprogenitor cells at the interface sense a motion-free and strain-free environment, which induces only a baseline level of osteogenesis.

This type of strain-free environment can be created when dental implants are submerged into the bones of the jaw and then covered with oral soft tissues [24]. Our findings suggest that loading an implant immediately after placement stimulates osseointegration (Fig. 5). There is, however, a caveat: we controlled the amount of loading to create moderate strains throughout most of the region around the implant with the exception of certain strain-concentrating regions at the implant surface (Fig. 6B, D, G and Fig. 7A, B). Whether immediate loading of dental implants creates moderate or excessive strains – or some combination of each – is not known; the answer will likely depend upon factors such as implant geometry and surface texture; the loads applied to the implant; the initial anchorage of the implant in bone; and the quality and quantity of the surrounding bone. Consequently, the sequelae of immediate loading can not be predicted at this time, although our findings point to an interplay between the factors listed above and the interfacial strain fields.

In orthopaedic situations almost every implant is, in effect, loaded. For example, elevation of the leg following a hip implant loads the implant stem. Does this type of loading constitute micromotion, and if so, does it create moderate effective strains that are osteogenic? Or does this modest movement of the extremity generate excessive strains that are detrimental to bone formation? Clearly, there is great utility in being able to define the mechanical environment around an implant, and then to understand how a specific mechanical environment influences cell behavior *in vivo*.

Strain fields of moderate magnitude represent areas of increased osteogenesis

In our mouse model, implant displacement profoundly affected bone formation in the cortical gap and in the bone marrow cavity. For example, on the periosteal side of the unloaded gap new bone formed through a cartilage intermediate whereas on the endosteal side of the gap, bone formed by the direct differentiation of skeletal progenitor cells into osteoblasts (Fig. 3).

Motion of the implant did not alter these programs of endochondral ossification on the periosteal surface, and intramembranous ossification on the endosteal surface; what was altered was the onset of osteogenesis, and the amount of bone that formed. When implants were subjected to a defined motion, exuberant bone formation was noted in both the gap and on the endosteal surface, and the initiation of this bone formation occurred earlier than in cases where the implant was stable. Relative to implant stabilization, why did implant displacement enhance osteogenesis? There are a number of *in vitro* studies that indicate shear stress initiates differentiation of osteoprogenitor cells into osteoblasts, but does not effect their proliferation [44,45]. The transfer of this knowledge to our data could help explain the earlier onset of bone formation in the loaded compared to the unloaded environment. On the other hand, it does not provide the answer for the exuberant bone formation. We found evidence that proliferative activity in tissues surrounding unloaded and loaded implant was equivalent (Leucht et al. 2006, submitted), so the difference in the amount of bone formed can not be solely attributed to increased proliferation. We speculate that micromotion serves as a stimulus to recruit osteochondroprogenitor cells from the surrounding tissue to the peri-implant region, much like morphogen gradients stimulate cell migration. Our strain measurements suggest that physical stimuli resulting from implant micromotion – such as strain fields – are distributed into the surrounding tissue. This mechanical perturbation results in up-regulation of osteogenic genes (Leucht et al. 2006, submitted), which eventually leads to bone matrix deposition. Therefore, the increase in bone mass surrounding the implant can be attributed to a wider propagation of osteogenic stimuli due the strain fields.

Does osseointegration recapitulate fracture healing?

While fracture healing and osseointegration are often-times represented as comparable processes. Both processes involve bone formation, and both are influenced by the mechanical environment. In fracture healing models, the mechanical environment can be exceedingly difficult to characterize. In addition, the healing regenerate is amorphous, which complicates molecular and histological analyses. In contrast, this model of osseointegration allows us to isolate, characterize, quantify, and ultimately influence how bone forms in a location-specific, highly reproducible manner around an implant. By controlling the mechanical force, measuring the strain fields, and correlating these with patterns of cell differentiation we can begin to understand how forces affect bone formation. We anticipate that this information will have direct relevance to understanding bone formation in a wide variety of clinical contexts, including fracture healing.

Acknowledgements

We would like to thank Daniel Nicolella, Kent Lam, and Yujin Park for their technical support. This work was funded by NIH grant: R01 EB000504-02 (JBB, AN, and JAH), FA9550-04-1-0075 (JAH)

References

1. Bechtold JE, Mouzin O, Kidder L, Soballe K. A controlled experimental model of revision implants: Part II. Implementation with loaded titanium implants and bone graft. Acta Orthop Scand 2001;72:650–656. [PubMed: 11817883]
2. Jones LC, Frondoza C, Hungerford DS. Effect of PMMA particles and movement on an implant interface in a canine model. J Bone Joint Surg Br 2001;83:448–458. [PubMed: 11341436]
3. Mouzin O, Soballe K, Bechtold JE. Loading improves anchorage of hydroxyapatite implants more than titanium implants. J Biomed Mater Res 2001;58:61–68. [PubMed: 11152999]
4. Skripitz R, Aspenberg P. Early effect of parathyroid hormone (1–34) on implant fixation. Clin Orthop Relat Res 2001:427–432. [PubMed: 11716418]
5. Toksvig-Larsen S, Jorn LP, Ryd L, Lindstrand A. Hydroxyapatite-enhanced tibial prosthetic fixation. Clin Orthop Relat Res 2000:192–200. [PubMed: 10660713]

6. Van der Vis HM, Aspenberg P, Marti RK, Tigchelaar W, Van Noorden CJ. Fluid pressure causes bone resorption in a rabbit model of prosthetic loosening. Clin Orthop Relat Res 1998:201–208. [PubMed: 9602821]
7. Willert HG, Buchhorn GH. Osseointegration of cemented and noncemented implants in artificial hip replacement: long-term findings in man. J Long Term Eff Med Implants 1999;9:113–130. [PubMed: 10537584]
8. Simmons CA, Meguid SA, Pilliar RM. Mechanical regulation of localized and appositional bone formation around bone-interfacing implants. J Biomed Mater Res 2001;55:63–71. [PubMed: 11426399]
9. Simmons CA, Meguid SA, Pilliar RM. Differences in osseointegration rate due to implant surface geometry can be explained by local tissue strains. J Orthop Res 2001;19:187–194. [PubMed: 11347689]
10. Clifford, DH., editor. Preanesthesia, anesthesia, analgesia, and euthanasia. New York: Academic Press; 1984. p. 527-562.
11. Sheehan, DC.; Hrapchak, BB. Theory and practice of Histotechnology. Columbus, Ohio: Batelle Press; 1980. p. 103-104.
12. Colnot C, Thompson Z, Miclau T, Werb Z, Helms JA. Altered fracture repair in the absence of MMP9. Development 2003;130:4123–4133. [PubMed: 12874132]
13. Albrecht, UEG.; Helms, JA.; Lin, H. Visualization of gene expression patterns by in situ hybridization. In: Daston, GP., editor. Molecular and cellular methods in developmental toxicology. Boca Raton, FL: CRC Press; 1997. p. 23-48.
14. Vogelin E, Jones NF, Huang JI, Brekke JH, Lieberman JR. Healing of a critical-sized defect in the rat femur with use of a vascularized periosteal flap, a biodegradable matrix, and bone morphogenetic protein. J Bone Joint Surg Am 2005;87:1323–1331. [PubMed: 15930543]
15. Malizos KN, Papatheodorou LK. The healing potential of the periosteum Molecular aspects. Injury 2005;36 (Suppl 3):S13–19. [PubMed: 16188544]
16. Ducy P. Cbfa1: a molecular switch in osteoblast biology. Dev Dyn 2000;219:461–471. [PubMed: 11084646]
17. Aubin JE. Bone stem cells. J Cell Biochem 1998;(Suppl 30–31):73–82.
18. Bell DM, Leung KK, Wheatley SC, Ng LJ, Zhou S, et al. SOX9 directly regulates the type-II collagen gene. Nature Genetics 1997;16:174–178. [PubMed: 9171829]
19. Akiyama H, Chaboissier MC, Martin JF, Schedl A, de Crombrugghe B. The transcription factor Sox9 has essential roles in successive steps of the chondrocyte differentiation pathway and is required for expression of Sox5 and Sox6. Genes Dev 2002;16:2813–2828. [PubMed: 12414734]
20. Einhorn TA. Clinically applied models of bone regeneration in tissue engineering research. Clin Orthop 1999:S59–67. [PubMed: 10546636]
21. Buckwalter JA. Effects of early motion on healing of musculoskeletal tissues. Hand Clinics 1996;12:13–24. [PubMed: 8655614]
22. Soballe K, Hansen ES, H BR, Jorgensen PH, Bunger C. Tissue ingrowth into titanium and hydroxyapatite-coated implants during stable and unstable mechanical conditions. J Orthop Res 1992;10:285–299. [PubMed: 1311039]
23. Wirtz DC, Heller KD, Niethard FU. [Biomechanical aspects of load-bearing capacity after total endoprosthesis replacement of the hip joint. An evaluation of current knowledge and review of the literature]. Z Orthop Ihre Grenzgeb 1998;136:310–316. [PubMed: 9795432]
24. Szmukler-Moncler S, Salama H, Reingewirtz Y, Dubruille JH. Timing of loading and effect of micromotion on bone-dental implant interface: review of experimental literature. J Biomed Mater Res 198;43:192–203. [PubMed: 9619438]
25. Kim DG, Brunski IB, Nicolella DP. Microstrain fields for cortical bone in uniaxial tension: optical analysis method. Proc Inst Mech Eng 2005;[H] 219:119–128.
26. Zhang L, Bail H, Mittlmeier T, Haas NP, Schaser KD. Immediate microcirculatory derangements in skeletal muscle and periosteum after closed tibial fracture. J Trauma 2003;54:979–985. [PubMed: 12777913]

27. Pazzaglia UE. Periosteal and endosteal reaction to reaming and nailing: the possible role of revascularization on the endosteal anchorage of cementless stems. Biomaterials 1996;17:1009–1014. [PubMed: 8736736]
28. Caplan AI. Cartilage. Sci Am 1984;251:84–87. 90–84. [PubMed: 6435245]
29. Caplan AI. Mesenchymal stem cells. J Orthop Res 1991;9:641–650. [PubMed: 1870029]
30. Muschler GF, Midura RJ. Connective tissue progenitors: practical concepts for clinical applications. Clin Orthop Relat Res 2002:66–80. [PubMed: 11937867]
31. Li M, Amizuka N, Oda K, Tokunaga K, Ito T, et al. Histochemical evidence of the initial chondrogenesis and osteogenesis in the periosteum of a rib fractured model: implications of osteocyte involvement in periosteal chondrogenesis. Microsc Res Tech 2004;64:330–342. [PubMed: 15481050]
32. Wilson SE, Mohan RR, Netto M, Perez V, Possin D, et al. RANK, RANKL, OPG, and M-CSF expression in stromal cells during corneal wound healing. Invest Ophthalmol Vis Sci 2004;45:2201–2211. [PubMed: 15223796]
33. Hazenberg JG, Freeley M, Foran E, Lee TC, Taylor D. Microdamage: A cell transducing mechanism based on ruptured osteocyte processes. J Biomech. 2005
34. Jones JI, Doerr ME, Clemmons DR. Cell migration: interactions among integrins, IGFs and IGFBPs. Prog Growth Factor Res 1995;6:319–327. [PubMed: 8817675]
35. Winkler DG, Sutherland MK, Geoghegan JC, Yu C, Hayes T, et al. Osteocyte control of bone formation via sclerostin, a novel BMP antagonist. Embo J 2003;22:6267–6276. [PubMed: 14633986]
36. Narayanan K, Ramachandran A, Hao J, He G, Park KW, et al. Dual functional roles of dentin matrix protein 1. Implications in biomineralization and gene transcription by activation of intracellular Ca2 + store. J Biol Chem 2003;278:17500–17508. [PubMed: 12615915]
37. Ajubi NE, Klein-Nulend J, Alblas MJ, Burger EH, Nijweide PJ. Signal transduction pathways involved in fluid flow-induced PGE2 production by cultured osteocytes. Am J Physiol 1999;276:E171–178. [PubMed: 9886964]
38. Cheng B, Kato Y, Zhao S, Luo J, Sprague E, et al. PGE(2) is essential for gap junction-mediated intercellular communication between osteocyte-like MLO-Y4 cells in response to mechanical strain. Endocrinology 2001;142:3464–3473. [PubMed: 11459792]
39. Zhang X, Schwarz EM, Young DA, Puzas JE, Rosier RN, et al. Cyclooxygenase-2 regulates mesenchymal cell differentiation into the osteoblast lineage and is critically involved in bone repair. J Clin Invest 2002;109:1405–1415. [PubMed: 12045254]
40. Claes LE, Heigele CA, Neidlinger-Wilke C, Kaspar D, Seidl W, et al. Effects of mechanical factors on the fracture healing process. Clin Orthop 1998;355:S132–147. [PubMed: 9917634]
41. Wong M, Siegrist M, Goodwin K. Cyclic tensile strain and cyclic hydrostatic pressure differentially regulate expression of hypertrophic markers in primary chondrocytes. Bone 2003;33:685–693. [PubMed: 14555274]
42. Carter, DR.; Beaupre, G. Skeletal tissue regeneration. Cambridge: Cambridge University Press; 2001. p. 161-200.
43. Henderson JH, Fuente LD, Romero D, Colnot CI, Huang S, et al. Rapid Growth of Cartilage Rudiments may Generate Perichondrial Structures by Mechanical Induction. Biomech Model Mechanobiol. 2006
44. Kreke MR, Goldstein AS. Hydrodynamic shear stimulates osteocalcin expression but not proliferation of bone marrow stromal cells. Tissue Eng 2004;10:780–788. [PubMed: 15265295]
45. Tanaka SM, Sun HB, Roeder RK, Burr DB, Turner CH, et al. Osteoblast responses one hour after load-induced fluid flow in a three-dimensional porous matrix. Calcif Tissue Int 2005;76:261–271. [PubMed: 15812578]

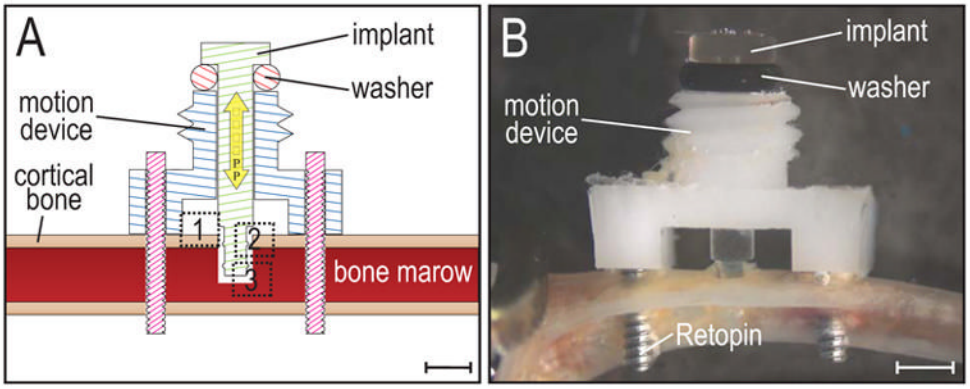

Figure 1.
Schematic illustration of implant and device.
(A) The motion device is positioned on the proximal tibia using two Ti-alloy Retopins®. The implant is guided through the middle of the motion device, and only penetrates one cortex. Note the geometry of the implant (a uniform cylinder with two circumferential ridges), which results in distinct strain patterns when the implant is axially displaced. **(B)** A cap (not shown) is screwed onto the motion device to hold the implant in place and secure it against accidental motion due to mouse activity. The cap contains a central hole, which allows a pin from an actuator (not shown) to create implant displacement without removing the cap. Dotted boxes represent the regions of interest (1: periosteum, 2: gap region, 3: bone marrow). Scale bar in A and B: 1mm.

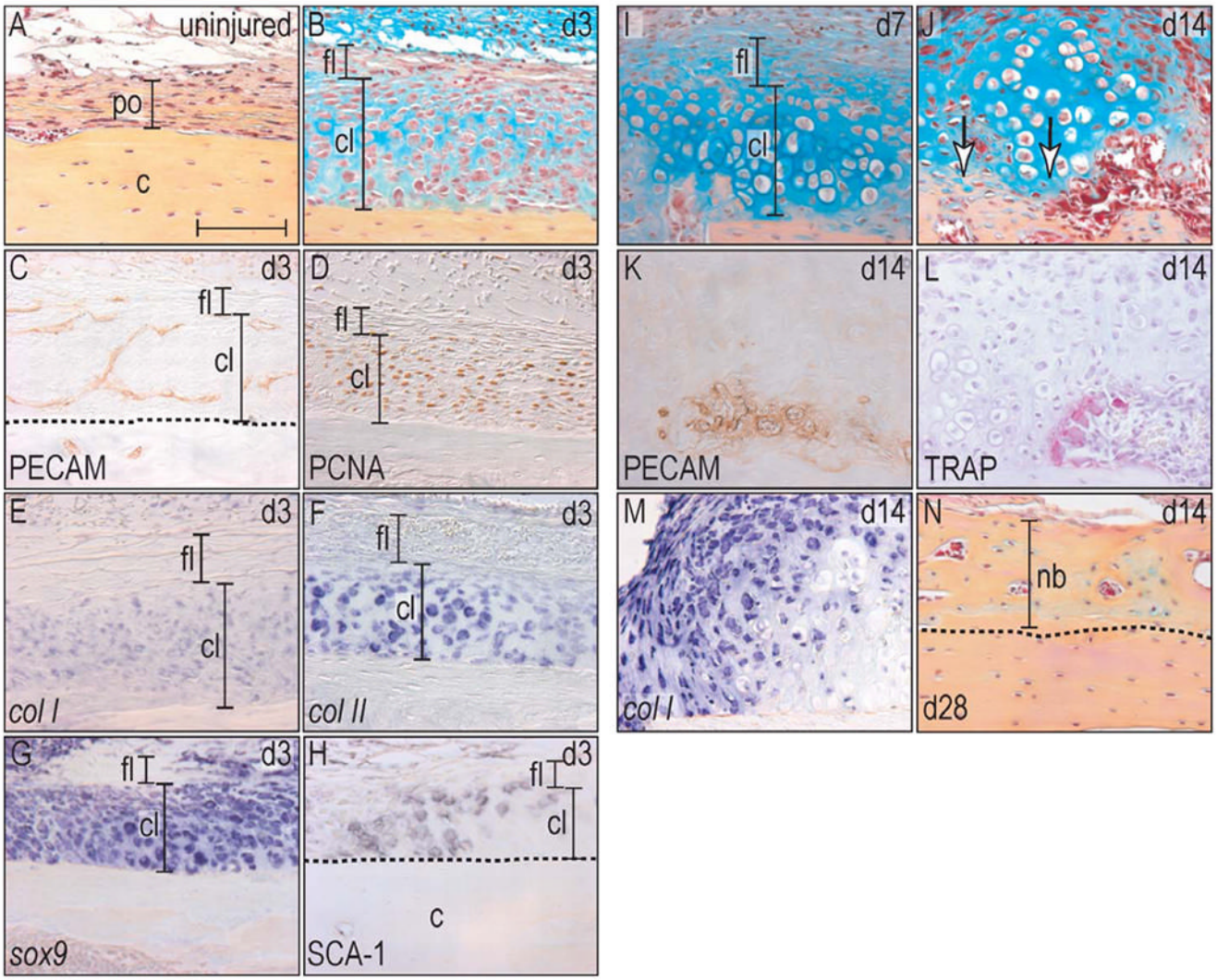

Figure 2.

Implant placement induces periosteal proliferation and finally endochondral bone formation. **(A)** Uninjured periosteum consists of a one cell layer thick cambial layer that is surrounded by a thicker fibrous layer. **(B)** At post-surgical day 3, the cambial layer has thickened almost tenfold, whereas the fibrous layer did not change histologically. **(C)** Newly formed vessels invaded into the cambial layer and created a capillary network. **(D)** PCNA-staining showed proliferative activity exclusively in the cambial layer. **(E–G)** *In situ* hybridization revealed that the proliferating cells were also positive for the osteochondroprogenitor cell marker *col I*, *col II*, *sox9*. **(H)** Sca-1 immunohistochemistry confirmed their osteoprogenitor capacity. **(I)** At post-surgical day 7, osteochondroprogenitor cells differentiated into chondrocytes with a subset showing signs of hypertrophy. **(J)** After 14 days, first signs of bone matrix deposition were evident (arrows), **(K)** and this mineralization was located close to newly formed vasculature. **(L)** Simultaneously with the deposition of a new bone matrix, TRAP positive osteoclasts started to remodel the newly deposited bone. **(M)** *Col I in situ* hybridization labeled the majority of cells in the periosteum, indicating their osteogenic potential, but was absent in hypertrophic chondrocytes. **(N)** At post-surgical day 28, the program of endochondral bone formation had finished and the new matrix was almost indistinguishable from the preexisting

cortical bone. Abbreviations: c: cortex; cl: cambial layer; fl: fibrous layer; nb: new bone; po: periosteum. Scale bar: 100 μm.

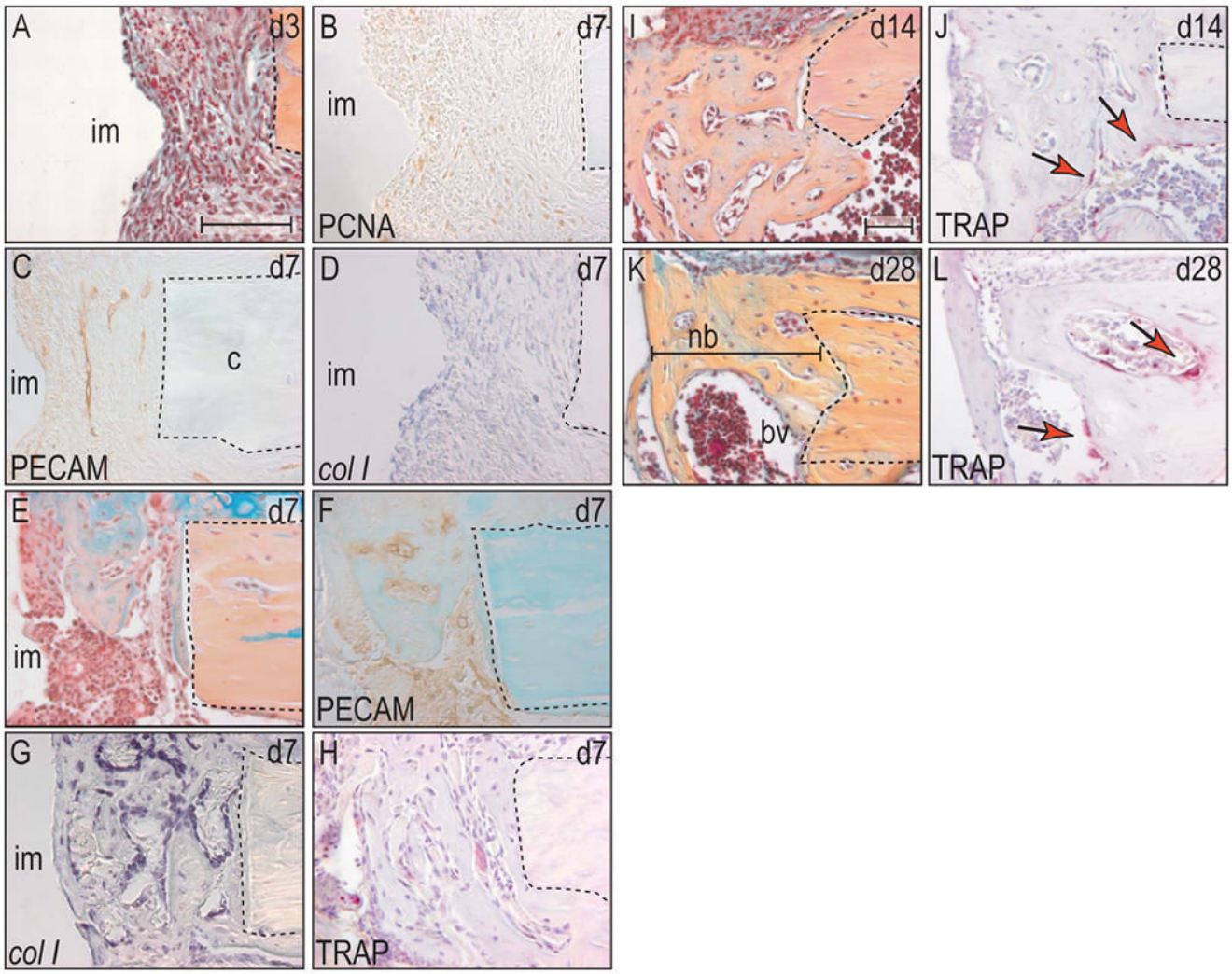

Figure 3.

Cortical gap is bridged by intramembranous bone formation.

(A) At post-surgical day 3, the gap was filled with a blood clot that was already invaded by fibroblasts. **(B)** PCNA-positive cells were primarily located at the circumferential ridges of the implant. **(C)** Angiogenesis occurred evenly throughout the gap area. **(D)** The expression pattern of *col I* co-localized with the area of high proliferative activity. **(E)** Seven days after surgery, intramembranous bone formation had already bridged ~50% of the gap. **(F)** This new bone matrix was deposited around the newly formed vessels that were already evident at post-surgical day 3. **(G)** *Col I* was exclusively expressed in osteoblast that aligned the woven bone matrix and in osteocytes, which were embedded in the matrix. **(H)** Again, TRAP positive osteoclasts started with the process of bone remodeling simultaneously with the onset of bone deposition. **(I)** At post-surgical day 14, the gap was completely filled with mature bone matrix, **(J)** which was still undergoing remodeling (arrows). **(K)** After 28 days, the border between preexisting bone and newly formed bone had almost faded. **(L)** Osteoclast activity was localized to vascular channels in the new bone matrix (arrows). Abbreviations: im: implant; bv: blood vessel; nb: new bone. Scale bar: 100 μm.

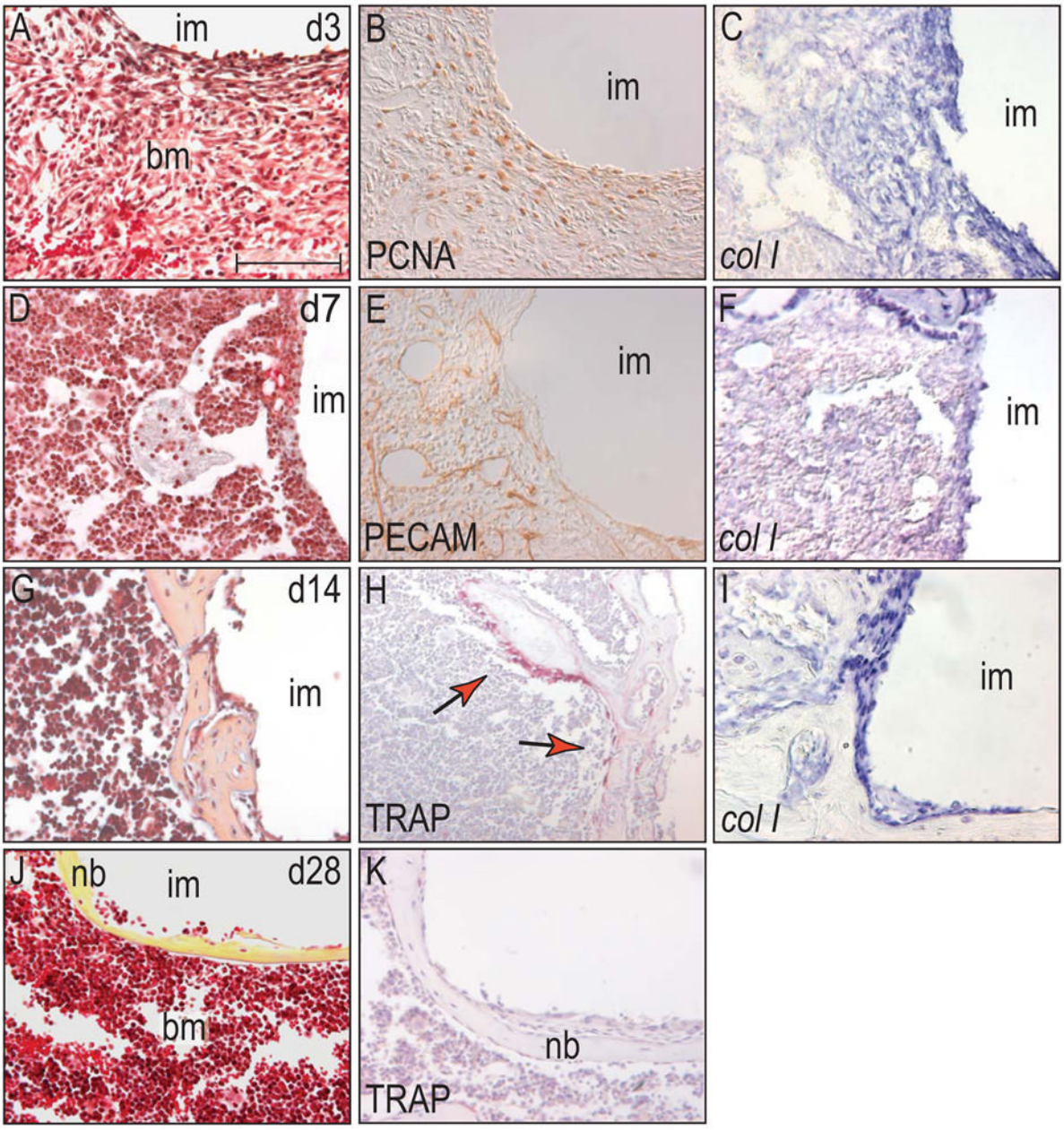

Figure 4.

Cells in the bone marrow cavity of a stable implant follow a similar but slower program of bone formation than cells in the cortical gap region.

(A) The wound site in the bone marrow cavity at day 3 was populated by spindle-shaped cells, without any evidence of bone matrix deposition. **(B)** Cells at the interface between implant and bone marrow exhibited high proliferative activity and **(C)** expressed the osteochondroprogenitor cell marker *col I* at high levels. **(D)** At post-surgical day 7, histology revealed that the interface was populated by cells with a similar morphology as bone marrow stromal cells without signs of matrix secretion. **(E)** PECAM-positive endothelial cells invaded the interface area and built a capillary network. **(F)** *Col I* expression was limited to a thin band around the implant. **(G)** Fourteen days after implant placement, a rough thin shell encapsulated

the base of the implant. **(H)** Once again, bone remodeling by osteoclasts started immediately when osteoblasts secreted a mineralized matrix. **(I)** Osteoblasts, which were attached to the bone matrix, were labeled by *col I in situ* hybridization. **(J)** After 28 days, the bony encapsulation of the implant was finished, resulting in a smooth thin layer of lamellar bone, **(K)** without any evidence of osteoclastic activity. Abbreviations: im: implant; bm: bone marrow. Scale bar: 100 μm.

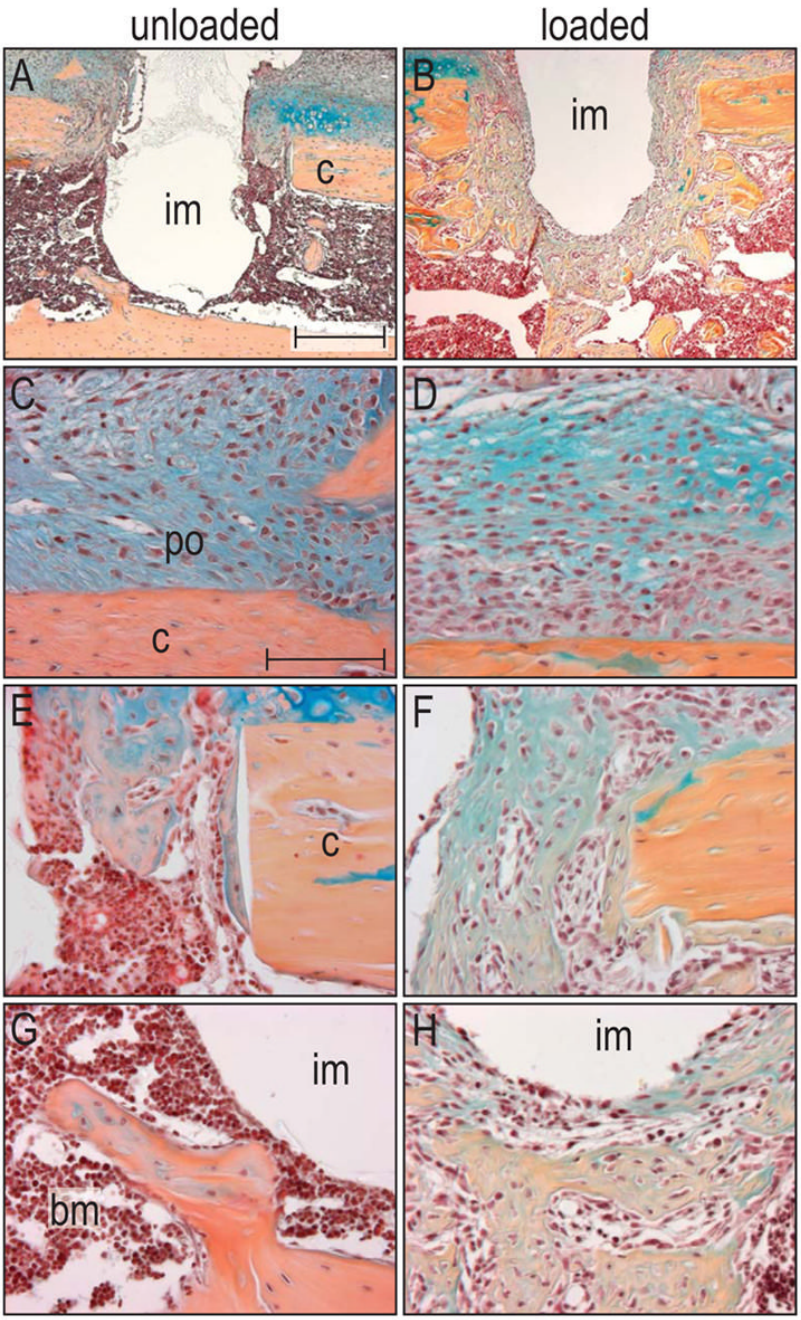

Figure 5.

Micromotion induces exuberant bone formation in gap and bone marrow compartments after seven days.

(A) Seven days after implant placement in an unloaded environment, bone formation only occurred in the gap region, but not in the bone marrow cavity. **(B)** In contrast, micromotion induced a dramatic increase in bone formation in the gap and bone marrow cavity. High magnification of the periosteum showed that in both the unloaded **(C)** and loaded cases **(D)**, cells started to proliferate and to differentiate into either chondrocytes or osteoblasts. **(E)** About half of the gap region in unloaded implants was filled with a bony matrix, **(F)** whereas micromotion resulted in a nearly complete osseous fill of the gap. **(G)** The bone marrow cavity

surrounding the unloaded implant lacked significant, newly deposited osseous matrix. **(H)** The most robust result accompanying a physical stimulus occurred in the marrow cavity, where exuberant bone formation encapsulated most of the implant. Abbreviations: b: bone marrow; c: cortex; im: implant; po: periosteum. Scale bar in A, B: 300 μm, C-H: 100 μm.

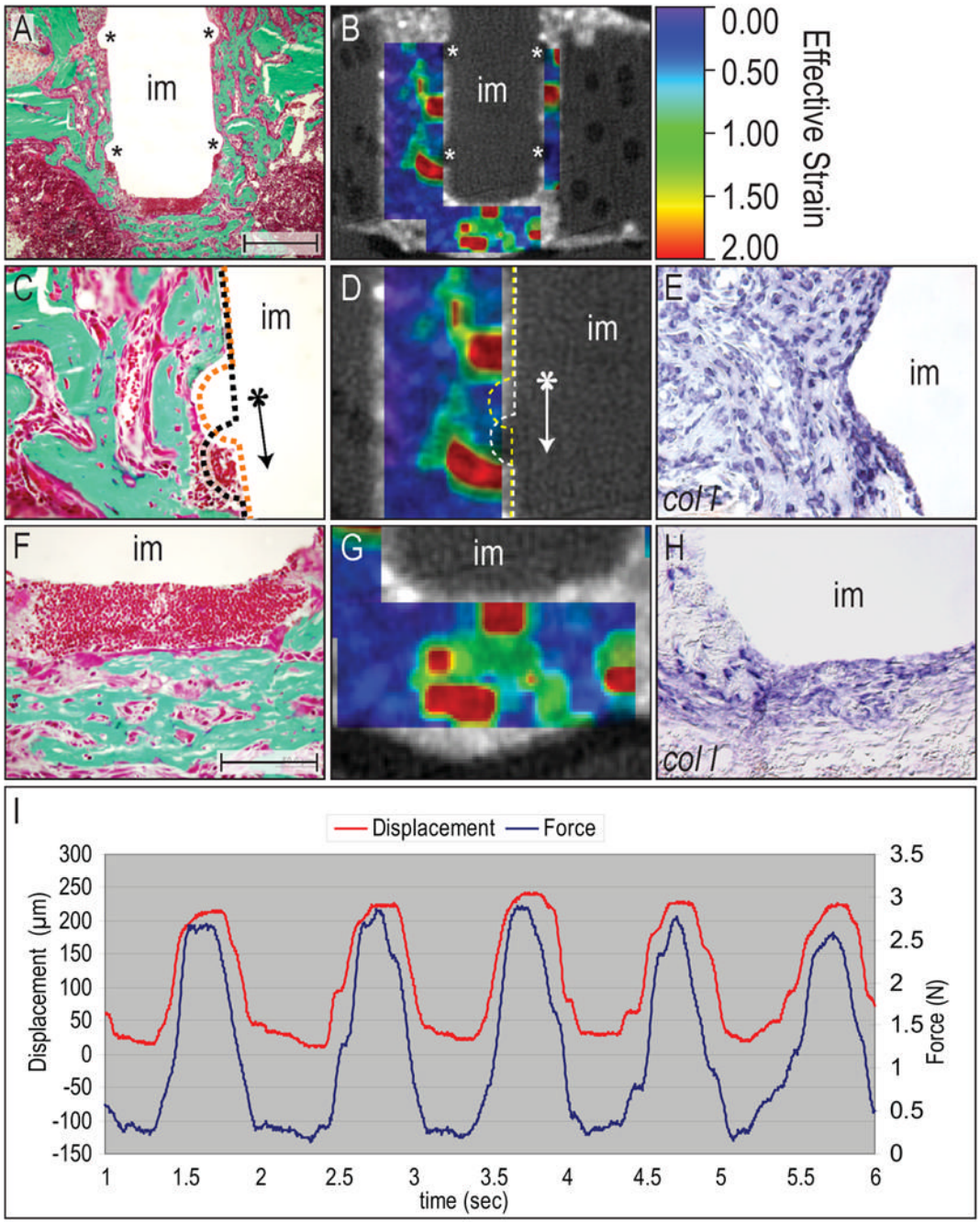

Figure 6.

Strain fields and their relation to tissue around the implant.

(A) Histology (Goldner's trichrome) showing the implant with circumferential ridges (asterisks). **(B)** Micro-CT image overlaid with contours of effective strain (which is $\epsilon_{eff} = \frac{2}{\sqrt{3}}(\epsilon_I^2 + \epsilon_{II}^2 + \epsilon_I\epsilon_{II})^{\frac{1}{2}}$, where ε_I and ε_{II} are the principal strains) enabled a correlation between the strain field and molecular and cellular analysis. **(C, D)** By comparing the histology with the magnitude of the effective strain, we were able to show a relationship between areas of excessively-large strains (1–2) with areas that did not exhibit matrix deposition. When the

implant was displaced (arrow), it created high strains underneath the ridges which eventually resulted in a regenerate that was comprised of fibroblasts and red blood cells, without mineralized matrix. **(E)** Despite lacking mineralized matrix, some of the cells in this area were expressing *col I*, indicating their osteogenic potential. **(F, G)** The mesenchyme surrounding the base of the implant was built of two distinct tissues that were shaped by the mechanical stimulus; soft tissue occupied a ~150μm thick area underneath the implant, which represented areas of highest strains. Further away, strain magnitude decreased and therefore allowed for osteoblast differentiation and eventually bone matrix deposition. **(H)** Again, cells in the area of excessive strains expressed the osteogenic marker *col I*, but did not differentiate into matrix-secreting osteoblasts. **(I)** Graph showing the displacement of the implant measured with a LVDT (red), and the force required to achieve this displacement (Load cell, blue). Abbreviations: im: implant. Scale bar in A, B: 300 μm, C-H: 100 μm.

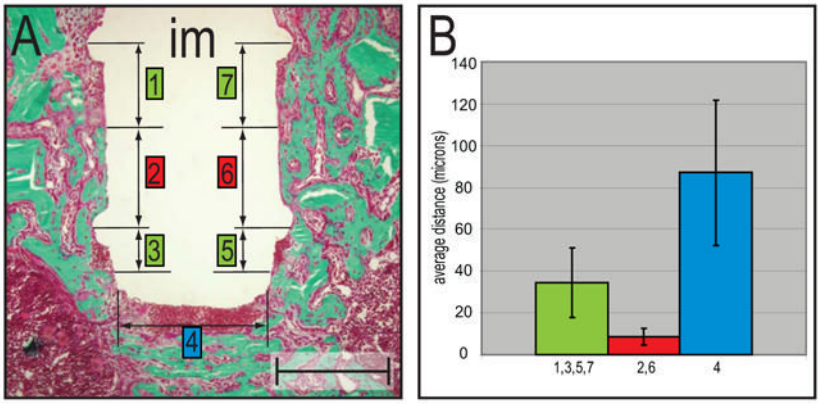

Figure 7.

Histomorphometry of bone matrix deposition at various implant locations.

(A) The tissue-implant interface (Goldner's trichrome) was divided into seven locations that represented areas of low (2,6) or high (1,7,3,4,5) effective strain fields. **(B)** The graph shows a difference in the distance between implant surface and bone matrix deposition in three areas. The areas of high effective strains (e.g., base of implant, tissue underneath circumferential ridges) revealed the greatest distance, while the area in between the ridges, which was subjected to moderate strains, showed bone formation in close proximity to the implant. Error bars show mean and standard deviations. Abbreviations: im: implant. Scale bar: 300 μm.